Nuclear Engineering and Design 238 (2008) 2292–2301

Contents lists available at ScienceDirect

Nuclear Engineering and Design

journal homepage: www.elsevier.com/locate/nucengdes

Solution of neutron transport equation using Daubechies' wavelet expansion in the angular discretization

Liangzhi Cao*, Hongchun Wu, Youqi Zheng

Department of Nuclear Engineering, Xi'an Jiaotong University, Xi'an, Shaanxi 710049, China

ARTICLE INFO

Article history:
Received 4 December 2007
Received in revised form 2 March 2008
Accepted 5 March 2008

ABSTRACT

Daubechies' wavelet expansion is introduced to discretize the angular variables of the neutron transport equation when the neutron angular flux varies very acutely with the angular directions. An improvement is made by coupling one-dimensional wavelet expansion and discrete ordinate method to make two-dimensional angular discretization efficient and stable. The angular domain is divided into several subdomains for treating the vacuum boundary condition exactly in the unstructured geometry. A set of wavelet equations coupled with each other is obtained in each subdomain. An iterative method is utilized to decouple the wavelet moments. The numerical results of several benchmark problems demonstrate that the wavelet expansion method can provide more accurate results by lower-order expansion than other angular discretization methods.

1. Introduction

Traditional angular approximate methods such as spherical harmonics (P_N) method and discrete ordinate (S_N) method have been utilized in the neutron transport calculation without fuel-coolant homogenization. Recent study (Smith, 2001) indicated that those traditional methods could not converge to the exact solutions unless high-order angular approximations are adopted in a pin cell calculation. Further study (Adams, 2001) found that the high-energy angular flux distribution in an infinite lattice of fuel and moderator is a bumpy and irregular function in the azimuthal direction by use of high-order S_N method. Hundreds of azimuthal points were needed to resolve the accurate solution. All these problems present great challenges to existing angular discretization schemes in heterogeneous neutron transport calculation. Additionally, high-precision angular flux calculation is also becoming more and more important in the nuclear applications. It is significantly and widely required in the radiation shielding, the arrangement of nuclear experiments and the nuclear medicine (Dang et al., 1999).

In recent decades, wavelet analysis theory has been well developed and widely applied in various fields. Daubechies (1992) constructed a series of wavelet functions named Daubechies' wavelet, which were proved (Dohon, 1993) to be unconditional bases in Banach space. Preliminary studies have demonstrated (Cho and Park, 1996; Cho and Cao, 2006) that wavelet analysis theory could be well used in the neutron transport solution. Compared with other wavelet basis (Carron, 1999; Buchan et al., 2005), Daubechies' wavelet basis owns obvious advantages due to the localization property and the picky performance. It is more flexible and effective in the high-precision approximation of complex functions. This property presents the possibility of expanding the angular variables of neutron transport equation into wavelet functions.

In this paper, Daubechies' wavelet basis is applied to expand the angular variables of one- and two-dimensional neutron transport equation. In order to increase the computational efficiency, an effective improvement is made by treating the polar variable and the azimuthal variable independently, *i.e.*, the polar variable is discretized by using traditional discrete ordinate method and the azimuthal variable is expanded into wavelet functions. This is mainly because that the angular flux does not suffer great change in the polar direction in most two-dimensional problems. This angular discretization scheme significantly decreases the scale of coupled moments in two-dimensional problems. It makes the wavelet expansion acceptable in high-order high-dimensional neutron transport calculation. The wavelet equations are then deduced in an angular subdomain scheme to use the vacuum boundary condition easily in the unstructured geometry. An over relaxation iterative scheme is utilized in decoupling the coupled wavelet moments.

The remainder of this paper is organized as follows. In Section 2, the wavelet expansion is introduced briefly. In Section 3, the wavelet equations in each angular subdomain are derived. In Section 4, corresponding solver scheme is given. In Section 5, results of several benchmark problems are discussed. Finally, in Section 6, conclusions are used to close the paper.

* Corresponding author. Tel.: +86 29 8266 3285; fax: +86 29 8266 7802.
E-mail address: caolz@mail.xjtu.edu.cn (L. Cao).

0029-5493/$ – see front matter © 2008 Elsevier B.V. All rights reserved.
doi:10.1016/j.nucengdes.2008.03.003

2. The preliminaries of wavelet expansion method

2.1. The definition and properties of Daubechies' wavelet function

The Daubechies' wavelet functions $w_{j,k}(x)$ are generated by a dilation and translation operation such as

$$w_{j,k}(x) = 2^{j/2} w(2^j x - k) \quad j, k \in Z, w \in L^2(R) \tag{1}$$

Z and R denote the set of integers and real numbers, respectively. $L^2(R)$ denotes the space of measurable, square-integrable functions.

The corresponding scaling functions in multi-resolution analysis (Daubechies, 1992) have the same forms:

$$\varphi_{j,k}(x) = 2^{j/2} \varphi(2^j x - k) \quad j, k \in Z, \varphi \in L^2(R) \tag{2}$$

Two-scale relations exist between wavelet functions and scaling functions as:

$$w(x) = \sqrt{2} \sum_k (-1)^{k-1} h_{N-k-1} \varphi(2x - k) \quad k = 0, N-1 \tag{3}$$

where N stands for Daubechies' order and h_{N-k-1} are Daubechies' coefficients.

The Daubechies' wavelet function $w_{j,k}(x)$ has the following properties:

$$\text{support}\,(w_{j,k}(x)) = [2^{-j}k, 2^{-j}(k + 2N - 1)] \tag{4}$$

$$\int w_{j,k}(x)\mathrm{d}x = 0 \qquad \int w_{n,k}(x) w_{m,l}(x)\mathrm{d}x = \delta_{mn}\delta_{kl} \tag{5}$$

Here j, n, m is called 'dilation order'. Eq. (4) shows us the supporting region is related to the dilation order and Daubechies' order. Compact supports vest the wavelet functions with localization property, which is very powerful in angular discretization. Eq. (5) shows the orthogonality of the wavelet functions. This property makes it possible to utilize wavelet function as the expansion basis in solving neutron transport equation.

The construction of Daubechies' scaling function $\varphi_{j,k}(x)$ begins with the coefficients h_k by two-scale equation:

$$\varphi(x) = \sqrt{2} \sum_{k=0}^{2N-1} h_k \varphi(2x - k) \tag{6}$$

From this equation, the values of Daubechies' scaling function at integers are calculated as an eigenvector. Values of the wavelet functions at other points can be recursively obtained from the two-scale relationship.

In order to simulate unknown functions, the Daubechies' wavelet function is usually limited to a unit interval so that all unknown functions are assumed to be defined only for the range [0,1). There are several methods to limit the wavelet function on [0,1) in wavelet analysis theory, here we chose the wrapped wavelet method (Newland, 1993). This method is an effective path of cyclic continuation by use of discrete values from Eqs. (3) and (6).

2.2. The decomposition and reconstruction of wavelet expansion

In this paper, Daubechies' wavelet is used in this form:

$$w_m(t) = w(2^{j-1}t - k) \quad m = 2^{j-1} + k, j = 1, \infty, k = 0, 2^{j-1} - 1 \tag{7}$$

and the wavelet expansion of a L^2 function $f(x)$ is written as:

$$f(x) = b_0 + \sum_j \sum_k b_{2^{j-1}+k} w(2^{j-1}x - k)$$

$$0 \le x < 1, j = 1, \infty, k = 0, 2^{j-1} - 1 \tag{8}$$

Fig. 1 illustrates the process that how wavelet works. Differing from other polynomial function expansion methods, the wavelet expansion consists of decomposition and reconstruction. Taking a bumpy function defined in Eq. (9) for example, the wavelet expansions of different expansion order divide the sample function into four levels, which are included in different basis. The average value is contained in the base level as shown in Fig. 1(a). Other levels of wavelet components in different frequency contribute to the exact distribution of the variable. They are illustrated in Fig. 1(b). By adding the separated wavelet components together, the sample function is reconstructed as shown in Fig. 1(c).

$$f(x) = \sin(8\pi x) + 2 \times \sin(12\pi x) \quad 0 \le x < 1 \tag{9}$$

The principle of wavelet decomposition and reconstruction supplies a very powerful instrument to exactly approximate the angular variables in neutron transport equation. Compared with traditional polynomial function expression methods such as P_N method, the wavelet expression method is efficient and high precision while the angular flux presents a complex distribution along with the angular variables.

3. Wavelet expansion of neutron transport equation

The first-order multi-group neutron transport equation can be written as

$$\Omega \nabla \phi_g(r, \Omega) + \Sigma_{t,g} \phi_g(r, \Omega) = Q_{f,g} + Q_{s,g} + S_g(r) \tag{10}$$

where Ω denotes the unit direction vector and the angular variable, r is the space variable.

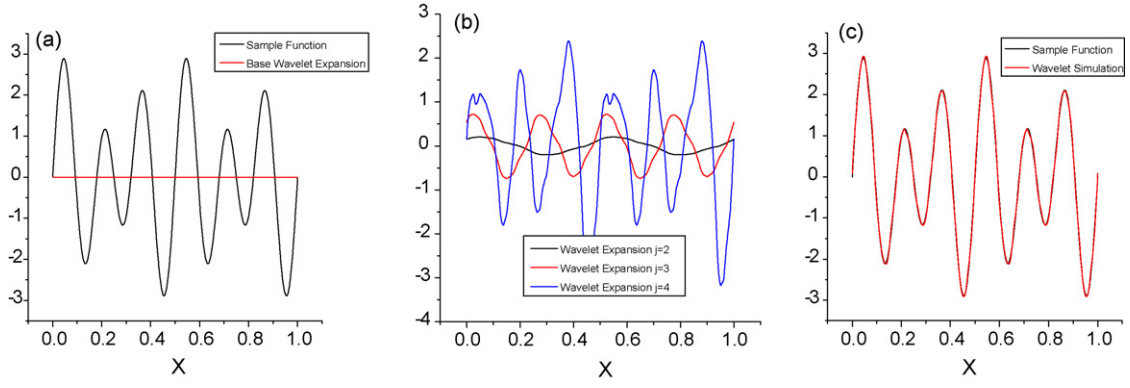

Fig. 1. (a–c) Decomposition and reconstruction of the sample function from Daubechies' wavelet.

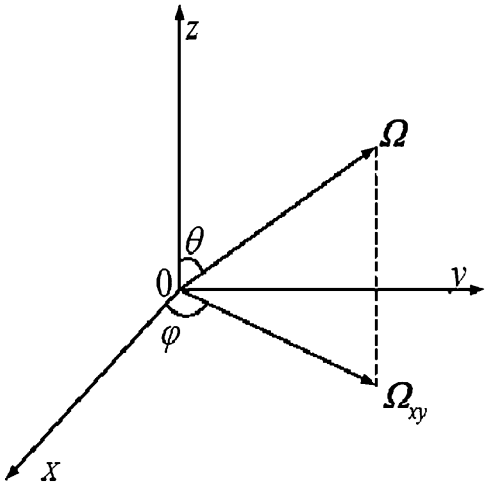

Fig. 2. Angle definition in Cartesian geometry.

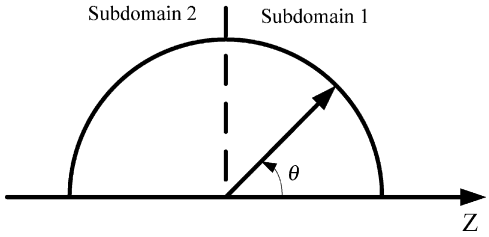

Fig. 3. Division of angular domain in one-dimensional case.

3.1. One-dimensional wavelet expansion

In one-dimensional case, neutron transport equation can be written as

$$\mu\frac{\partial\phi_g}{\partial z}(z,\mu)+\Sigma_{t,g}\phi_g(z,\mu)=Q_{f,g}+Q_{s,g}+S_g(z) \tag{11}$$

The Cartesian geometry discussed here is shown in Fig. 2. μ denotes the polar cosine($\cos\theta$)as shown in Fig. 2. Only isotropic scattering is considered. The fission source and the scattering source can be presented as Eqs. (12) and (13), respectively. Only isotropic scattering is considered in this study:

$$Q_{f,g}=\frac{\chi_g}{2k}\sum_{g'=1}^{G}\int_{-1}^{1}\nu\Sigma_{f,g'}\phi_{g'}(z,\mu')\mathrm{d}\mu' \tag{12}$$

$$Q_{s,g}=\frac{1}{2}\sum_{g'=1}^{G}\int_{-1}^{1}\Sigma_s^{g'-g}\phi_{g'}(z,\mu')\mathrm{d}\mu' \tag{13}$$

As a function expansion method, the treatment of vacuum boundary condition is also a puzzle in the wavelet expansion. Here an angular subdomain scheme is introduced into the wavelet expansion. By expanding the angular variable in each angular subdomain, the vacuum boundary condition can be solved directly. In one-dimensional case, the angular subdomain is divided into two regions spontaneously as in Fig. 3.

Then, the neutron transport equation can be written as follows:

$$\mu\frac{\partial\phi_g^1(z,\mu)}{\partial z}+\Sigma_{t,g}\phi_g^1(z,\mu)=Q_{f,g}^1+Q_{s,g}^1+S_g^1(z) \tag{14}$$

$$-\mu\frac{\partial\phi_g^2(z,-\mu)}{\partial z}+\Sigma_{t,g}\phi_g^2(z,-\mu)=Q_{f,g}^2+Q_{s,g}^2+S_g^2(z) \tag{15}$$

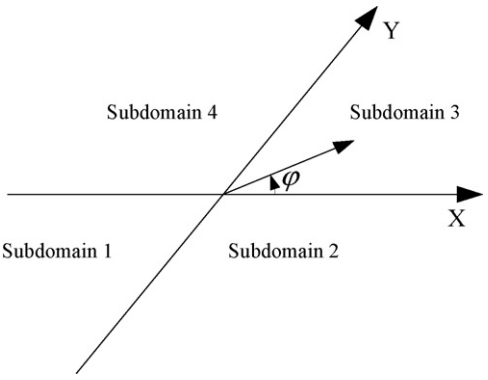

Fig. 4. Division of angular domain in two-dimensional case.

where $\mu\in[0,1)$. Expand the angular flux by use of wavelet basis as

$$\phi_g(z,\mu)=\sum_n\psi_{g,n}(z)w_n(\mu) \tag{16}$$

Substitute Eqs. (14) and (15) by Eq. (16), respectively, the wavelet equations in each angular subdomain can be written as

$$\sum_n\left[\mu\frac{\partial\psi_{g,n}^1(z)w_n(\mu)}{\partial z}+\Sigma_{t,g}\psi_{g,n}^1(z)w_n(\mu)\right]=Q_{f,g}^1+Q_{s,g}^1+S_g^1(z) \tag{17}$$

$$\sum_n\left[-\mu\frac{\partial\psi_{g,n}^2(z)w_n(\mu)}{\partial z}+\Sigma_{t,g}\psi_{g,n}^2(z)w_n(\mu)\right]=Q_{f,g}^2+Q_{s,g}^2+S_g^2(z) \tag{18}$$

Then, apply the Galerkin method to solve the above equations. The weighting functions are also chosen to be the wavelet basis, *i.e.*, $w_n(\mu)$. After multiplying an individual wavelet basis on both sides and integrating in the angular subdomains, we obtain the following equations by using the orthogonality property of Daubechies' wavelet function:

$$\sum_n A_{nn'}\frac{\partial\psi_{g,n}^1(z)}{\partial z}+\Sigma_{t,g}\psi_{g,n'}^1(z)=Q_{f,g,n'}^1+Q_{s,g,n'}^1+S_{g,n'}^1(z) \tag{19}$$

$$\sum_n -A_{nn'}\frac{\partial\psi_{g,n}^2(z)}{\partial z}+\Sigma_{t,g}\psi_{g,n'}^2(z)=Q_{f,g,n'}^2+Q_{s,g,n'}^2+S_{g,n'}^2(z) \tag{20}$$

where $n'=1\sim P_n$ and $A_{nn'}=\int_0^1\mu w_n(\mu)w_{n'}(\mu)\mathrm{d}\mu$. P_n denotes the total number of expansion coefficients of the polar variable. $\psi_{g,n}^1$ and $\psi_{g,n}^2$ stand for the wavelet expansion coefficients in each angular subdomain.

3.2. Two-dimensional wavelet expansion

The two-dimensional neutron transport equation can be written as

$$\sqrt{1-\mu^2}\cos\varphi\frac{\partial\phi_g(x,y,\mu,\varphi)}{\partial x}+\sqrt{1-\mu^2}\sin\varphi\frac{\partial\phi_g(x,y,\mu,\varphi)}{\partial y}+\Sigma_{t,g}\phi_g(x,y,\mu,\varphi)=Q_{f,g}+Q_{s,g}+S_g(x,y) \tag{21}$$

μ denotes the polar cosine and φ stands for the azimuthal variable as shown in Fig. 2. Fig. 4 illustrates the division of angular subdomain in two-dimensional case. Then, the neutron transport equation can be written as follows:

$$\sqrt{1-\mu^2}\cos(-\pi+\varphi)\frac{\partial\phi_g^1(x,y,\mu,-\pi+\varphi)}{\partial x} + \sqrt{1-\mu^2}\sin(-\pi+\varphi)\frac{\partial\phi_g^1(x,y,\mu,-\pi+\varphi)}{\partial y} + \Sigma_{t,g}\phi_g^1(x,y,\mu,-\pi+\varphi) = Q_{f,g}^1 + Q_{s,g}^1 + S_g^1(x,y) \quad (22)$$

$$\sqrt{1-\mu^2}\cos(-\varphi)\frac{\partial\phi_g^2(x,y,\mu,-\varphi)}{\partial x} + \sqrt{1-\mu^2}\sin(-\varphi)\frac{\partial\phi_g^2(x,y,\mu,-\varphi)}{\partial y} + \Sigma_{t,g}\phi_g^2(x,y,\mu,-\varphi) = Q_{f,g}^2 + Q_{s,g}^2 + S_g^2(x,y) \quad (23)$$

$$\sqrt{1-\mu^2}\cos\varphi\frac{\partial\phi_g^3(x,y,\mu,\varphi)}{\partial x} + \sqrt{1-\mu^2}\sin\varphi\frac{\partial\phi_g^3(x,y,\mu,\varphi)}{\partial y} + \Sigma_{t,g}\phi_g^3(x,y,\mu,\varphi) = Q_{f,g}^3 + Q_{s,g}^3 + S_g^3(x,y) \quad (24)$$

$$\sqrt{1-\mu^2}\cos(\pi-\varphi)\frac{\partial\phi_g^4(x,y,\mu,\pi-\varphi)}{\partial x} + \sqrt{1-\mu^2}\sin(\pi-\varphi)\frac{\partial\phi_g^4(x,y,\mu,\pi-\varphi)}{\partial y} + \Sigma_{t,g}\phi_g^4(x,y,\mu,\pi-\varphi) = Q_{f,g}^4 + Q_{s,g}^4 + S_g^4(x,y) \quad (25)$$

where $\mu \in [0,1)$ and $\varphi \in [0, \pi/2)$.

The wavelet expansion can be applied in a two-dimensional function $f(x, y)$ by tensor product construction in the same way as one-dimensional case. It is shown in following equation:

$$f(x,y) = \sum_m\sum_n c_{mn}w_{mn}(x,y) = \sum_m\sum_n c_{mn}w_m(x)w_n(y) \quad (26)$$

Based on it, the wavelet expansion of angular flux in two-dimensional case can be written as:

$$\phi_g(x,y,\mu,\varphi) = \sum_m\sum_n \psi_{g,mn}(x,y)w_m(\mu)w_n(\xi), \quad \xi = \frac{2}{\pi}\varphi \quad (27)$$

Substitute Eqs. (22)–(25) by Eq. (27) and utilize the same method given in Section 3.1, the wavelet equations in each angular subdomain can be obtained as follows:

$$\sum_m\sum_n\left[-A_{mm'nn'}\frac{\partial\psi_{g,mn}^1(x,y)}{\partial x} - B_{mm'nn'}\frac{\partial\psi_{g,mn}^1(x,y)}{\partial y}\right] + \Sigma_{t,g}\psi_{g,m'n'}^1(x,y) = Q_{f,g,m'n'}^1 + Q_{s,g,m'n'}^1 + S_{g,m'n'}^1(x,y) \quad (28)$$

$$\sum_m\sum_n\left[A_{mm'nn'}\frac{\partial\psi_{g,mn}^2(x,y)}{\partial x} - B_{mm'nn'}\frac{\partial\psi_{g,mn}^2(x,y)}{\partial y}\right] + \Sigma_{t,g}\psi_{g,m'n'}^2(x,y) = Q_{f,g,m'n'}^2 + Q_{s,g,m'n'}^2 + S_{g,m'n'}^2(x,y) \quad (29)$$

$$\sum_m\sum_n\left[A_{mm'nn'}\frac{\partial\psi_{g,mn}^3(x,y)}{\partial x} + B_{mm'nn'}\frac{\partial\psi_{g,mn}^3(x,y)}{\partial y}\right] + \Sigma_{t,g}\psi_{g,m'n'}^3(x,y) = Q_{f,g,m'n'}^3 + Q_{s,g,m'n'}^3 + S_{g,m'n'}^3(x,y) \quad (30)$$

$$\sum_m\sum_n\left[-A_{mm'nn'}\frac{\partial\psi_{g,mn}^4(x,y)}{\partial x} + B_{mm'nn'}\frac{\partial\psi_{g,mn}^4(x,y)}{\partial y}\right] + \Sigma_{t,g}\psi_{g,m'n'}^4(x,y) = Q_{f,g,m'n'}^4 + Q_{s,g,m'n'}^4 + S_{g,m'n'}^4(x,y) \quad (31)$$

where $m' = 1 \sim P_m$, $n' = 1 \sim P_n$ and $A_{mm'nn'} = \int_0^1 \sqrt{1-\mu^2}w_m(\mu)w_{m'}(\mu)\mathrm{d}\mu \int_0^1 \cos(\pi/2\xi)w_n(\xi)w_{n'}(\xi)\mathrm{d}\xi$ $B_{mm'nn'} = \int_0^1 \sqrt{1-\mu^2}w_m(\mu)w_{m'}(\mu)\mathrm{d}\mu \int_0^1 \sin(\pi/2\xi)w_n(\xi)w_{n'}(\xi)\mathrm{d}\xi$. P_m and P_n denote the total number of expansion coefficients of the polar variable and azimuthal variable, respectively. $\psi_{g,mn}^1$, $\psi_{g,mn}^2$, $\psi_{g,mn}^3$, $\psi_{g,mn}^4$ stand for the wavelet expansion coefficients in each angular subdomain.

It can be seen that there are $2^{J_m+J_n}$ coupled wavelet moments need to be solved in Eqs. (28)–(31). J_m and J_n stand for the expansion order of the polar variable and azimuthal variable, respectively. According to the numerical test experience which will be given in Section 5.2, this amount of unknowns requires large computational steps, sometimes unacceptable in two-dimensional calculation even though the expansion order is not so high. It necessitates the improvement in two-dimensional wavelet expansion.

Previous studies indicate the transport solution of the angular flux distribution is relatively smooth in the polar direction in most two-dimensional problems (Adams, 2001). This phenomenon illumes the idea of treating the polar variable and azimuthal variable independently. A new angular discretization scheme is therefore raised based on the tensor product form of two-dimensional wavelet expansion in Eq. (26). In this scheme, the wavelet basis is only used to expand the azimuthal variable and a traditional discrete ordinate method is used to deal with the polar variable.

Define $\int_{\Delta\mu_m}\phi_g(r,\mu,\varphi)\mathrm{d}\mu = \omega_m\phi_{g,m}(r,\varphi)$ and $\int_{\Delta\mu_m}\Omega\nabla\phi_g(r,\mu,\varphi)\mathrm{d}\mu = \omega_m[\Omega\nabla\phi_g(r,\mu,\varphi)]_m$.

The wavelet equations in each angular subdomain are rewritten as

$$\sqrt{1-\mu_m^2}\left[\cos(-\pi+\varphi)\frac{\partial\phi_{g,m}^1(x,y,-\pi+\varphi)}{\partial x} + \sin(-\pi+\varphi)\frac{\partial\phi_{g,m}^1(x,y,-\pi+\varphi)}{\partial y}\right] + \Sigma_{t,g}\phi_{g,m}^1(x,y,-\pi+\varphi) = Q_{f,g,m}^1 + Q_{s,g,m}^1 + S_{g,m}^1(x,y) \quad (32)$$

$$\sqrt{1-\mu_m{}^2}\left[\cos(-\varphi)\frac{\partial\phi_{g,m}^2(x,y,-\varphi)}{\partial x} + \sin(-\varphi)\frac{\partial\phi_{g,m}^2(x,y,-\varphi)}{\partial y}\right] + \Sigma_{t,g}\phi_{g,m}^2(x,y,-\varphi) = Q_{f,g,m}^2 + Q_{s,g,m}^2 + S_{g,m}^2(x,y) \quad (33)$$

$$\sqrt{1-\mu_m{}^2}\left[\cos\varphi\frac{\partial\phi_{g,m}^3(x,y,\varphi)}{\partial x} + \sin\varphi\frac{\partial\phi_{g,m}^3(x,y,\varphi)}{\partial y}\right] + \Sigma_{t,g}\phi_{g,m}^3(x,y,\varphi) = Q_{f,g,m}^3 + Q_{s,g,m}^3 + S_{g,m}^3(x,y) \quad (34)$$

$$\sqrt{1-\mu_m{}^2}\left[\cos(\pi-\varphi)\frac{\partial\phi_{g,m}^4(x,y,\pi-\varphi)}{\partial x} + \sin(\pi-\varphi)\frac{\partial\phi_{g,m}^4(x,y,\pi-\varphi)}{\partial y}\right] + \Sigma_{t,g}\phi_{g,m}^4(x,y,\pi-\varphi) = Q_{f,g,m}^4 + Q_{s,g,m}^4 + S_{g,m}^4(x,y) \quad (35)$$

The corresponding wavelet basis is defined as

$$\phi_{g,m}(x,y,\varphi)=\sum_n \psi_{g,mn}(x,y)w_n(\xi),\quad \xi=\frac{2}{\pi}\varphi \tag{36}$$

Thus,

$$\sqrt{1-\mu_m^2}\sum_n\left[-A_{nn'}\frac{\partial\psi^1_{g,mn}(x,y)}{\partial x}-B_{nn'}\frac{\partial\psi^1_{g,mn}(x,y)}{\partial y}\right]+\Sigma_{t,g}\psi^1_{g,mn'}(x,y)=Q^1_{f,g,mn'}+Q^1_{s,g,mn'}+S^1_{g,mn'}(x,y) \tag{37}$$

$$\sqrt{1-\mu_m^2}\sum_n\left[A_{nn'}\frac{\partial\psi^2_{g,mn}(x,y)}{\partial x}-B_{nn'}\frac{\partial\psi^2_{g,mn}(x,y)}{\partial y}\right]+\Sigma_{t,g}\psi^2_{g,mn'}(x,y)=Q^2_{f,g,mn'}+Q^2_{s,g,mn'}+S^2_{g,mn'}(x,y) \tag{38}$$

$$\sqrt{1-\mu_m^2}\sum_n\left[A_{nn'}\frac{\partial\psi^3_{g,mn}(x,y)}{\partial x}+B_{nn'}\frac{\partial\psi^3_{g,mn}(x,y)}{\partial y}\right]+\Sigma_{t,g}\psi^3_{g,mn'}(x,y)=Q^3_{f,g,mn'}+Q^3_{s,g,mn'}+S^3_{g,mn'}(x,y) \tag{39}$$

$$\sqrt{1-\mu_m^2}\sum_n\left[-A_{nn'}\frac{\partial\psi^4_{g,mn}(x,y)}{\partial x}+B_{nn'}\frac{\partial\psi^4_{g,mn}(x,y)}{\partial y}\right]+\Sigma_{t,g}\psi^4_{g,mn'}(x,y)=Q^4_{f,g,mn'}+Q^4_{s,g,mn'}+S^4_{g,mn'}(x,y) \tag{40}$$

where $m'=1\sim M$ and $n'=1\sim P_n$, M denotes the total number of Gaussian points determined in traditional S_N method in the polar direction and P_n stands for the total number of expansion coefficients of the azimuthal variable.

Compared with direct two-dimensional wavelet expansion, the discrete ordinate wavelet expansion decreases the number of coupled wavelet moments from 2^{Jm+Jn} to 2^{Jn} for each fixed polar variable. Numerical result given in Section 5.2 demonstrates that this improved angular discretization scheme removed most coupled unknown wavelet moments while the accuracy is still good enough. It makes high-order two-dimensional calculations much more efficiency.

As the angular flux always varies slowly in the polar direction in most two-dimensional problems and we only use discrete ordinate discretization in the polar variable, ray effect, which always occurs in the S_N method, does not appear in this method.

4. The solution of wavelet equations

4.1. The iterative method for coupled wavelet equations

There are many unknown wavelet moments which are coupled strongly with each other by a set of partial differential equations. The finite difference method may be an ideal method with the step scheme. However, due to the objective in heterogeneous neutron transport calculation, the least-square finite element method (Wu and Ju, 2007) for first-order neutron transport equation is selected to solve the coupled partial differential equations in this study and a corresponding iterative method is introduced into the solution.

Regarding $\psi_{g,mn'}(x,y)$ as unknown and the other moments as known for any given m and n', it is very convenient to get the decoupled wavelet equations in each angular subdomain. Taking the wavelet equations in the first angular subdomain as an example, we can get:

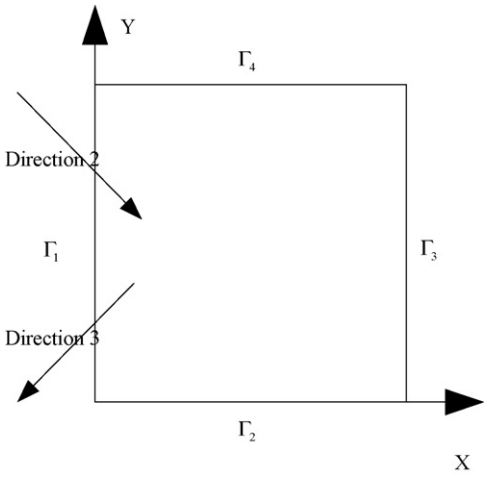

Fig. 5. Boundary definition in typical geometry.

$$\sqrt{1-\mu_m^2}\left[-A_{n'n'}\frac{\partial\psi^{1,k+1}_{g,mn'}(x,y)}{\partial x}-B_{n'n'}\frac{\partial\psi^{1,k+1}_{g,mn'}(x,y)}{\partial y}\right]+\Sigma_{t,g}\psi^{1,k+1}_{g,mn'}(x,y)=Q^{1,k}_{g,mn'}+F^{1,k}_{n'}(x,y) \tag{41}$$

where

$$Q^{1,k}_{g,mn'}=Q^{1,k}_{f,g,mn'}+Q^{1,k}_{s,g,mn'}+S^{1,k}_{g,mn'}(x,y) \tag{42}$$

and

$$F^{1,k}_{n'}(x,y)=\sqrt{1-\mu_m^2}\sum_{n\neq n'}\left[A_{nn'}\frac{\partial\psi^{1,k}_{g,mn}(x,y)}{\partial x}+B_{nn'}\frac{\partial\psi^{1,k}_{g,mn}(x,y)}{\partial y}\right] \tag{43}$$

To make the iteration stable, an over relaxation method is applied. Thus, Eq. (41) can be rewritten as

$$\sqrt{1-\mu_m^2}\left[-A_{n'n'}\frac{\partial\psi^{1,k+1}_{g,mn'}(x,y)}{\partial x}-B_{n'n'}\frac{\partial\psi^{1,k+1}_{g,mn'}(x,y)}{\partial y}\right]+\Sigma_{t,g}\psi^{1,k+1}_{g,mn'}(x,y)=Q^{1,k}_{g,mn'}+(1+\omega)F^{1,k}_{n'}(x,y)-\omega F^{1,k-1}_{n'}(x,y) \tag{44}$$

where ω is the over relaxation factor, which depends on the size of meshes. Corresponding to the over relaxation method, an additional iteration is resolved in each angular subdomains for several times before each step in the source iterations. A series of tests are taken to certificate the stabilization of the iteration with different Daubechies' order and expansion order. The numerical results given in Section 5 will show the iterative method can solve the coupled wavelet equations effectively and accurately.

4.2. The treatments of boundary conditions

Two types of boundary conditions are considered in this paper. Considering a traditional geometry as shown in Fig. 5, we take the Γ_1 boundary as an example.

a. Vacuum boundary condition

The definition of vacuum boundary condition is

$$\phi_g(r_b,\Omega)=0,\quad \Omega\cdot n<0 \tag{45}$$

In the Γ_1 side, the angular flux in the second angular subdomain is considered as the incident angular flux.Considering

$$\left\langle \phi^2_{g,m}\left(r_b, -\frac{\pi}{2}\xi\right), \quad w_{n'}(\xi)\right\rangle = \left\langle \sum_n \psi^2_{g,mn}(r_b) w_n(\xi), \quad w_{n'}(\xi)\right\rangle = 0 \tag{46}$$

The vacuum boundary condition expression in the Γ_1 side is obtained as

$$\psi^2_{g,mn}(r_b) = 0 \tag{47}$$

b. Reflective boundary condition

The definition of reflective boundary condition is

$$\phi_g(r_b, \Omega) = \phi_g(r_b, \Omega') \tag{48}$$

In the Γ_1 side, the angular flux in the second angular subdomain is considered as the incident angular flux corresponding to the emergent angular flux in the third angular subdomain. Thus, the reflective boundary condition can be written as

$$\phi^2_{g,m}\left(r_b, -\frac{\pi}{2}\xi\right) = \phi^3_{g,m}\left(r_b, \frac{\pi}{2}\xi\right) \tag{49}$$

Considering,

$$\left\langle \phi^2_{g,m}\left(r_b, -\frac{\pi}{2}\xi\right), \quad w_{n'}(\xi)\right\rangle = \left\langle \sum_n \psi^2_{g,mn}(r_b) w_n(\xi), \quad w_{n'}(\xi)\right\rangle = \left\langle \phi^3_{g,m}\left(r_b, \frac{\pi}{2}\xi\right), \quad w_{n'}(\xi)\right\rangle = \left\langle \sum_n \psi^3_{g,mn}(r_b) w_n(\xi), \quad w_{n'}(\xi)\right\rangle \tag{50}$$

The reflective boundary condition expression in the Γ_1 side is obtained as

$$\psi^2_{g,mn}(r_b) = \psi^3_{g,mn}(r_b) \tag{51}$$

The other angular subdomains in each side (Γ_2, Γ_3 and Γ_4) are treated analogously. Then the decoupled wavelet equations could be solved easily subdomain by subdomain.

5. The numerical results

A multi-group transport calculation code, WAVFEM, is developed according to the method described above. It can be used to solve both fixed source problems and eigenvalue problems in arbitrary geometry with different Daubechies' order and expansion order. It also provides an option of choosing direct wavelet expansion or discrete ordinate wavelet expansion in two-dimensional calculations. The unstructured meshes are generated by use of the general FEM software ANSYS. Several benchmark problems considering only isotropic scattering are calculated using this code. The angular flux is reconstructed in all two-dimensional calculations. Due to the smooth distribution of angular flux in the polar direction in two-dimensional problems, we focus only on the angular flux distribution in the azimuthal direction by applying the discrete ordinate expansion.

5.1. Reed cell benchmark problem

This problem is a one-dimensional five regions fixed source problem given by Buchan et al. (2005). It is chosen to verify the accuracy of the wavelet expansion over complex condition shown in Fig. 6. The cross-sections in each region are shown in Table 1. Reflective boundary condition and vacuum boundary are applied in the left and the right side, respectively.

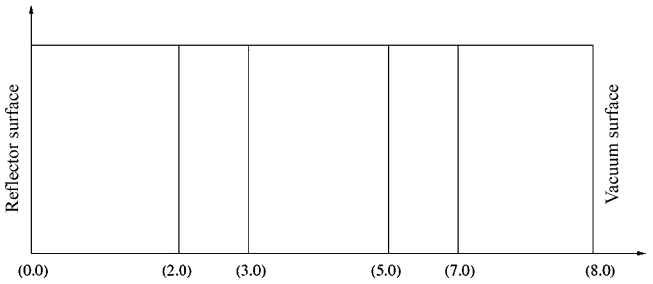

Fig. 6. Geometry of Reed cell benchmark.

Table 1
The cross-section of Reed cell benchmark

	Source ($cm^{-2}\ s^{-1}$)	Σ_t (cm^{-1})	Σ_s (cm^{-1})
Region 1	50.0	50.0	0.0
Region 2	0.0	5.0	0.0
Region 3	0.0	0.0	0.0
Region 4	1.0	1.0	0.9
Region 5	0.0	1.0	0.9

The scalar flux distribution is shown in Fig. 7, from which we can see the scalar flux suffers significant change in region 2 and region 4. Four results are presented with expansion order $J = 0, 1, 2, 3$, respectively. The result given by Buchan with P_9 approximation is taken as reference (Buchan et al., 2005). It is easy to find that the result of WAVFEM with expansion order $J = 2$ is very close to that of P_9. There are, however, only 4 coupled unknown moments are needed in the wavelet expansion in each angular subdomain, which is much less than that of P_9 with 10 coupled unknown moments.

5.2. One-dimensional Issa benchmark problem

This problem is a one-dimensional two regions eigenvalue problem designed by Issa et al. (1986). One-dimensional wavelet expansion, two-dimensional direct wavelet expansion and discrete ordinate wavelet expansion are all tested in this problem. The geometry is illustrated in Fig. 8 and the cross-sections are shown in Table 2. Reflective boundary condition and vacuum boundary condition are applied in the left and the right side, respectively. Additionally, in the two-dimensional calculations, reflective boundary condition is given both in the top and the base side, and the height of the regions is set to be 1 cm.

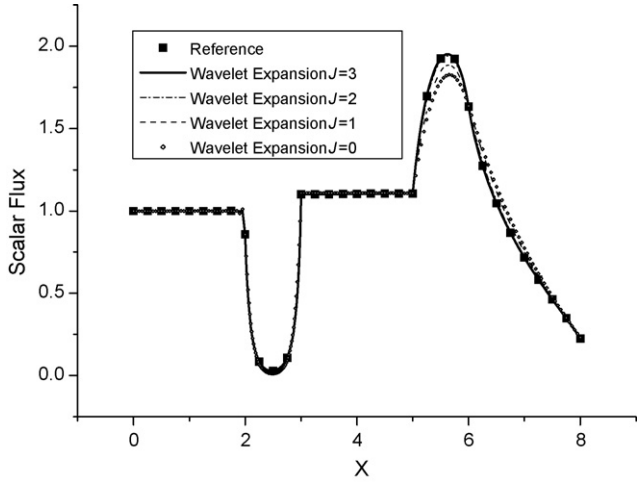

Fig. 7. Scalar distribution in Reed cell benchmark.

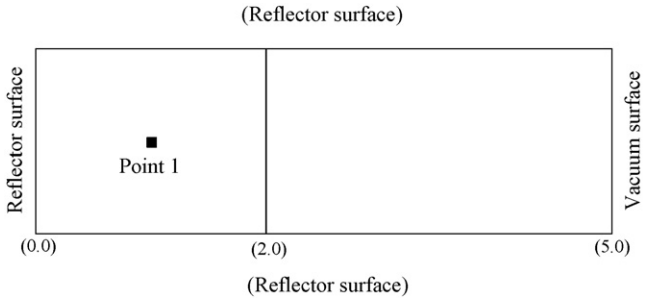

Fig. 8. Geometry of Issa benchmark.

Table 2
Cross-sections of Issa benchmark

	Σ_t (cm^{-1})	$\nu\Sigma_f$ (cm^{-1})	Σ_s (cm^{-1})
Region 1	1.0	1.0	0.5
Region 2	0.8	0.0	0.4

Table 3
Eigenvalues based on different methods of Issa benchmark

	Eigenvalue[a]
MCNP	1.6791
ANISIN S_{16}	1.6784
One-dimensional wavelet expansion	1.6805
Two-dimensional direct expansion	1.6804
Two-polar discrete ordinate wavelet expansion	1.6808

[a] All calculations based on the expansion order $J=4$ and Daubechies' order $N=3$.

The eigenvalues calculated by WAVFEM with different methods are shown in Table 3. They are compared with the result given by the one-dimensional S_N code ANISIN (Engle, 1973). Meanwhile, a precise reference is calculated by use of MCNP code (Briesmeister, 2002) with 400 generation and 50,000 particles in each generation. As described in Section 3.2, the number of unknown wavelet moments is determined by the expansion order. Take expansion order $J=3$ for example, there are 2^{3+3} coupled unknown moments in the wavelet equations by direct expansion method but only 2^3 coupled unknown moments at each fixed polar cosine by discrete ordinate expansion. Table 4 illustrates other comparisons between the two methods. The results demonstrate the efficiency of discrete ordinate wavelet expansion, which is very important in high-order high-dimensional calculations.

Based on different methods, Fig. 9 shows that all wavelet calculations reach high precision by increasing the order of expansion. Fig. 10 illustrates the scalar flux distribution in the base side. The reference value is obtained from code FELTRAN (Issa et al., 1986), which is based on the finite element spherical harmonics method.

In order to demonstrate the validity of high-precision angular flux simulation by use of the wavelet expansion, the angular flux distribution is reconstructed. The expansion order here is chosen as $J=4$. The result is compared with that of a least-square FEM S_N code LESFES with S_{16} discretization (Wu and Ju, 2007). Both codes

Table 4
Comparison of coupled unknown moments in different expansion

	$J=1$	$J=2$	$J=3$	$J=4$
Direct expansion				
Eigenvalue	1.6980	1.6870	1.6823	1.6804
No. of coupled moments	4	16	64	256
Two-polar discrete ordinate expansion				
Eigenvalue	1.6965	1.6884	1.6834	1.6808
No. of coupled moments	2×2	2×4	2×8	2×16

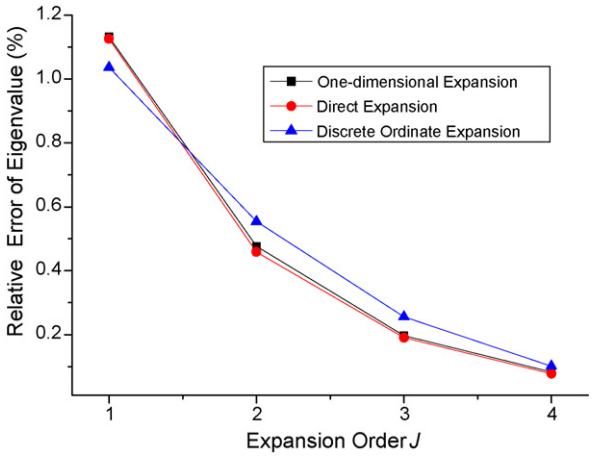

Fig. 9. Relative error of eigenvalues with different expansion order.

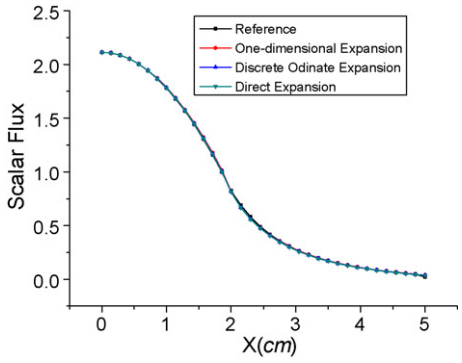

Fig. 10. Scalar flux distribution in the base side.

employ the same spatial discretization method. All calculations are based on the same 52 quadratic triangular meshes. Further refinement presents no visibly difference. Fig. 11 illustrates the angular flux distribution in the azimuthal direction at Point 1, which is shown in Fig. 8. The fixed polar variable is selected as $\mu=0.149$, where 32 discrete values of angular flux can be obtained from S_{16} discretization. The result presents well agreements with high-order S_N discretization in the wavelet expansion calculation, which could supply the angular flux at arbitrary angular point.

It is noticeable that visible discontinuity occurs in the adjacent regions of angular subdomains. It is an inevitable phenomenon

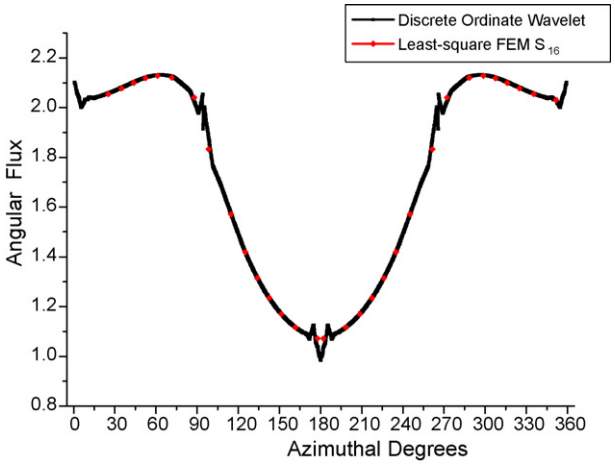

Fig. 11. Angular flux in the azimuthal dimension at fixed polar.

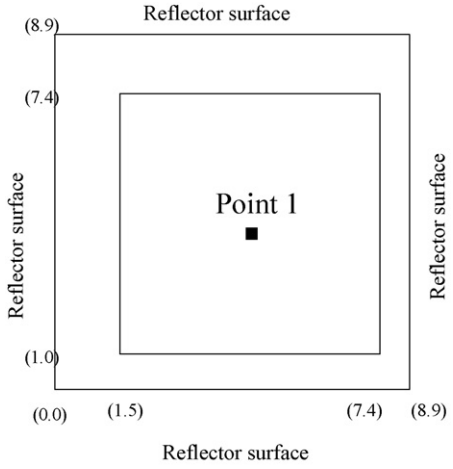

Fig. 12. Geometry of BWR cell benchmark.

called 'edge effect' in wavelet analysis theory. This is due to the use of wrapped Daubechies' wavelet expansion (Newland, 1993) in the angular subdomain scheme. It forces the values at edges of unknown functions to be equal according to cyclic continuation. According to the angular subdomian division in this study, it may cause the discontinuation shown in Fig. 11. Fortunately, numerical results show that the effect region of this phenomenon is very small while the expansion order is high and the effect could be negligible in the scalar flux calculations and eigenvalue calculations. Meanwhile, it should be specially mentioned that this problem is the most severe case in which edge effect occurs. It is due to the monotone change of angular flux in each angular subdomain, which does not occur frequently in neutron transport calculations.

5.3. Two-dimensional BWR cell benchmark problem

This problem is a two-dimensional two regions two-group eigenvalue problem designed by Stepanek et al. (1983) from a BWR cell. Region 1 stands for the homogeneous pin and region 2 denotes the moderator. The geometry is shown in Fig. 12 and the cross-sections are given in Table 5. Reflective boundary conditions are given in all sides.

The eigenvalues and normalized averaged scalar flux calculated by WAVFEM are given in Table 6. The reference is calculated by a neutron transport code SURCU (Stepanek et al., 1983) based on the integral transport theory. Clearly, calculations with a few fixed polar variables and low-order expansion reach enough precision. Meanwhile, the least-square FEM S_N code is calculated in this problem with the same 78 quadratic triangular meshes. The comparison in Fig. 13 shows that the wavelet expansion performs better precision while the same spatial discretization scheme is applied in this problem. However, much less unknown moments are required in the wavelet expansions, which make the calculation efficient potentially.

Table 5
Cross-sections of BWR cell benchmark

	$\nu\Sigma_f$ (cm^{-1})	$\Sigma_{1\to1}$ (cm^{-1})	$\Sigma_{1\to2}$ (cm^{-1})	Σ_t (cm^{-1})	χ
Group 1					
Fuel	6.203E−3	1.78E−1	1.002E−2	1.96647E−1	1.0
Moderator	0.0	1.995E−1	2.188E−2	2.22064E−1	
Group 2					
Fuel	1.101E−1	1.089E−3	5.255E−1	5.96159E−1	0.0
Moderator	0.0	1.558E−3	8.783E−1	8.87874E−1	

Table 6
Results of BWR cell benchmark

	Group 1		Group 2		Eigenvalue
	Fuel	Moderator	Fuel	Moderator	
Reference	1.0[a]	0.9269	0.3527	0.4514	1.2127
Discrete ordinate wavelet expansion					
2 polar and $J=2$	1.0	0.9380	0.3553	0.4601	1.2134
2 polar and $J=3$	1.0	0.9361	0.3548	0.4597	1.2133
3 polar and $J=2$	1.0	0.9331	0.3543	0.4565	1.2133
3 polar and $J=3$	1.0	0.9310	0.3538	0.4561	1.2132

[a] The average scalar flux in group 1 and fuel region is normalized to be unit.

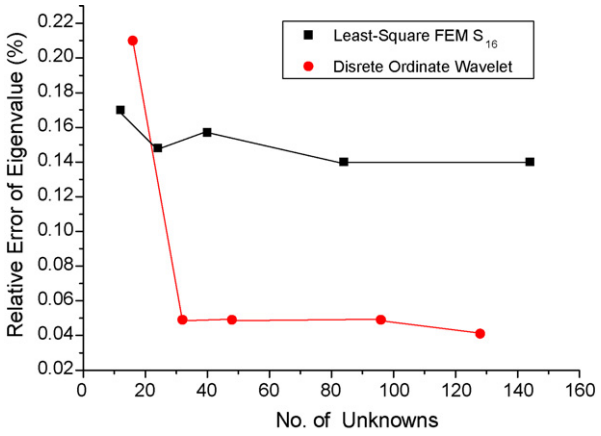

Fig. 13. Relative error of eigenvalue according to No. of unknowns.

The angular flux is reconstructed at the spatial point shown in Fig. 12 and fixed polar cosine $\mu = 0.149$. Fig. 14 illustrates the comparison of results from wavelet expansion with $J = 3$ and S_{16} angular discretization. The distribution of angular flux in the azimuthal direction is bumpy and peaky. It might be a reason why wavelet expansion gets more exact results in this problem. Suppose higher-order angular discretization would well improve the angular flux simulation in the S_N method. However, compared with the value of scalar flux, the amplitude of angular flux distribution is not obvious, *i.e.*, the angular flux distribution does not contribute much to the result of scalar flux calculation. Thus, traditional low-order angular approximations also reach good results in previous studies. Meanwhile, due to the non-monotonic change of angular flux, the

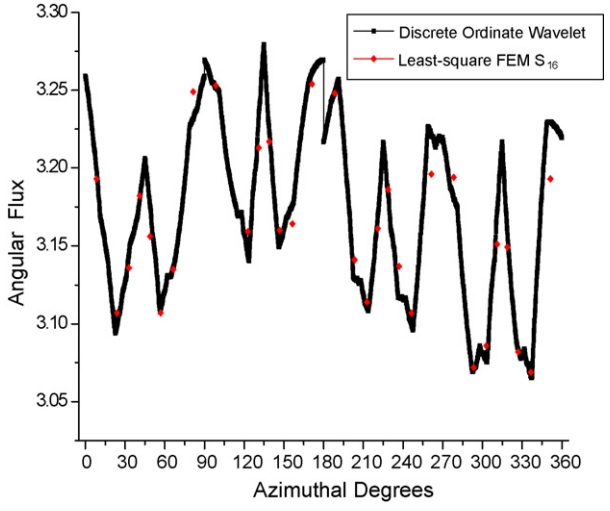

Fig. 14. Angular flux in the azimuthal dimension at fixed polar.

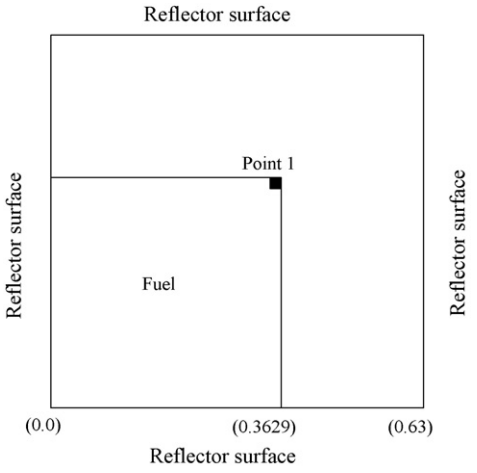

Fig. 15. Geometry of Adams's problem.

Table 7
Cross-section of Adams's problem

	Source ($cm^{-2}\,s^{-1}$)	Σ_t (cm^{-1})	Σ_s (cm^{-1})
Fuel	2π	0.141367	0.057843
Moderator	0.0	0.072774	0.008642

edge effect mentioned above is feeble in this problem as shown in Fig. 14.

5.4. Bumpy angular flux distribution reconstruction

This problem is based on an unexpected discovery by Adams (2001). It is a two regions fixed source problem focused on the high-energy flux. The geometry is shown in Fig. 15 and the cross-sections are given in Table 7. Reflective boundary conditions are given in all sides.

To demonstrate the accuracy of wavelet expansion, the results of MCNP code (Briesmeister, 2002) with 100,000,000 particles is selected as the reference. The average scalar flux agrees well with the reference as shown in Table 8. Fig. 16 gives a photocopy of the angular flux distribution given by Adams (2001). The result is obtained by use of a 'product' quadrature set with 512 uniformly spaced points in the azimuthal direction. It shows a solution of quite complexity of angular flux distribution in the azimuthal direction for a fixed polar cosine 0.33 at the spatial point shown in Fig. 15. The angular flux is reconstructed by use of wavelet expansion with Daubechies' order $N=3$ and expansion order $J=4$ for a fixed polar cosine 0.5774 according to the Gauss quadrature set in WAVFEM. The result is illustrated in Fig. 17. Compared with the reference, the angular flux presents similar distribution which is impossible to be simulated in other polynomial function expansion methods. Differences may be caused by different methods for polar variable selection and the angular subdomain scheme used in WAVFEM. However, there are only 16 coupled unknown moments in each angular subdomain to be determined, which is much less than the 512 points in the azimuthal variable according to Adams' work. Namely, the discrete ordinate wavelet expansion makes such calculation acceptable.

Table 8
Average scalar flux of Adams's problem

Average Scalar Flux	MCNP	Wavelet, $J=4$	Relative error (%)
Fuel	30.39	29.86	1.74
Moderator	28.99	29.25	0.90

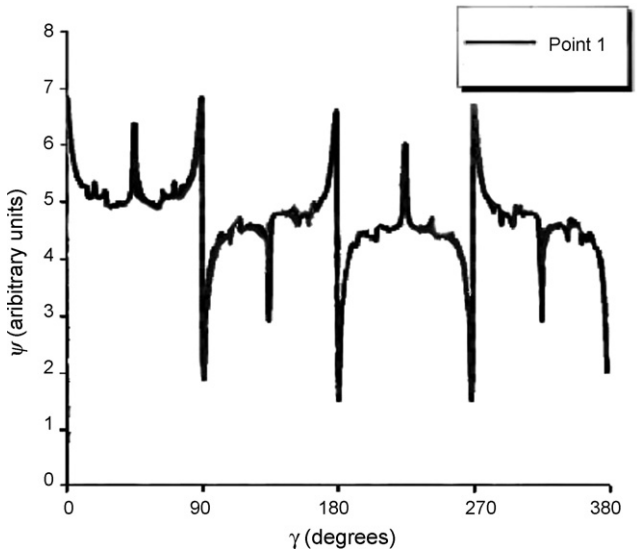

Fig. 16. Photocopy of angular flux distribution in Adams's problem (Adams, 2001).

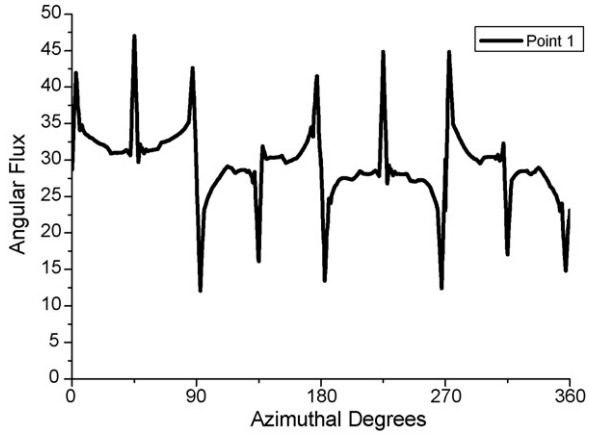

Fig. 17. Angular flux distribution obtained from wavelet expansion.

6. Conclusions

This paper uses the wavelet basis to expand the angular variable of first-order neutron transport equation and use the FEM to discretize the spatial variables on unstructured-meshes. Based on high-dimensional wavelet construction theory, an improved angular discretization scheme coupled of wavelet expansion and discrete ordinate method is introduced into two-dimensional calculation, which realizes the high-order high-dimensional wavelet expansion calculations in the neutron transport solutions. An iterative method is utilized to decouple the unknown moments of wavelet expansions with the application of an angular subdomain scheme. Numerical results demonstrate that the accuracy and flexibility of the wavelet expansion method are very good especially for the case with surged angular flux, and the iterative strategy is effective. Also, they show the advantages in high-order angular approximation with less unknown wavelet moments needed.

However, the edge effect arises in the angular subdomain scheme. It possibly causes the discontinuation of angular flux in

the adjacent regions of subdomains in some cases. Meanwhile, the least-square FEM is used to discretize the spatial variables in this paper. It costs much of the CPU time. Obviously, it can be substituted by any better method to save calculation time.

Acknowledgement

This research was carried out under the financial support of the National Science Foundation of China (Approved number 10605017).

References

Adams, M.L., 2001. Angular dependence of the fast flux in reactor lattices. Trans. Am. Nucl. Soc. 81, 212–214.

Briesmeister J.F., 2002. MCNP—A General Monte Carlo N-Particle Transport Code, Version 4C, LA-13709-M.

Buchan, A.G., Pain, C.C., et al., 2005. Linear and quadratic octahedral wavelets on the sphere for angular discretisations of the Boltzmann transport equation. Ann. Nucl. Energy 32, 1224–1273.

Cho, N.Z., Park, C.J., 1996. Wavelet theory for solution of the neutron diffusion equation. Nucl. Sci. Eng. 124, 417–430.

Cho, N.Z., Cao, L., 2006. Wavelet-theoretic method for solution of neutron transport equation. In: Transactions of the Korean Nuclear Society Spring Meeting, Chuncheon, Korea, May 25–26.

Carron, I., 1999. Solving the transport equation with spline wavelets. Technical Report, Dep. of Nuclear Eng., Texas, A&M University, College Station, Texas.

Dang, B., Wei, Z., et al., 1999. Determination of neutron angular distribution induced by 75 MeV/u12C ion beam in radiobiological experiment area. Radiat. Protec. 19, 140–143.

Daubechies, I., 1992. Ten Lectures on Wavelets. SIAM, Philadelphia, PA.

Dohon, D.L., 1993. Unconditional bases are optimal bases for data compression and for statistical. Appl. Comput. Harmonic Anal. 1 (1), 100–115.

Engle, W.W., 1973. A User's Manual for ANISN. USAEC Report KI-1693 (1967); ANISN-ORNL, A One-Dimensional Discrete Ordinates Transport Code. Oak Ridge National Laboratory Report CCC-254.

Issa, J.G., Riyait, N.S., Goddard, A.J.H., et al., 1986. Multigroup application of the anisotropic FEM code FELTRAN to one, two, three-dimensional and R-Z problems. Prog. Nucl. Eng. 18 (1), 251–264.

Newland, D.E., 1993. An Introduction to Random Vibrations, Spectral & Wavelet Analysis. John Wiley and Sons, New York.

Smith, M.A., 2001. Comparison of angular approximations for PWR cell calculations. Trans. Am. Nucl. Soc. 84, 90–91.

Stepanek, J., Auerbach, T., Haelg W., 1983. Calculation of four thermal reactor benchmark problems in X-Y geometry. EPRI NP-2855.

Wu, H., Ju, H., 2007. A least-square finite-element SN method for solving first-order neutron transport equation. Nucl. Eng. Des. 237, 823–829.